Electrogenerated Chemiluminescence of Pure Polymer Films and Polymer Blends[a]

Jiun-Tai Chen,* Ya-Lan Chang, Song Guo, Omar Fabian, William M. Lackowski, Paul F. Barbara

We recently reported the discovery of soliton-like electrogenerated chemiluminescence (ECL) waves from pure conjugated polymer films and gold-nanoparticles-doped polymer films. In addition to a more detailed study of these polymer systems by changing the film thickness and the distribution of local leaks, we also apply the ECL wave phenomenon to polymer blends of conjugated and nonconjugated polymers. Poly(9,9-dioctylfluorene-*co*-benzothiadiazole) (F8BT) is used as the active material that is oxidized and produces ECL with the presence of a co-reactant, tri-*n*-propylamine (TPA). Several factors such as film thickness, artificial leaks, and solubility of doped polymers are examined for their effects on the ECL behavior. When polystyrene (PS), less soluble in the electrolyte, is blended with F8BT, dotted ECL signals are observed and transported as waves. When poly(methyl methacrylate) (PMMA), more soluble in the electrolyte, is blended with F8BT, PMMA serves as local scratches and ECL waves are triggered simultaneously from the whole film.

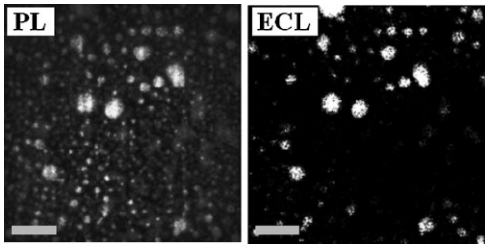

Introduction

Electrogenerated chemiluminescence (ECL) has aroused considerable interests among researchers in the fields of chemistry, analytical science, and nanotechnology because of its applications in various areas such as sensors and luminescence devices.[1–3] Many new materials have been studied during the development of ECL research. Among them, conjugated polymers are considered to be an important class of materials because of their unique electronic and optical properties.[4–6] But ECL studies of conjugated polymers are still relatively unexplored. In addition, some anomalous properties that have been observed in the electrochemical switching of conjugated polymers still fail to be explained.[7] Recently we have reported the discovery of soliton-like ECL waves from conjugated polymers using pure polymer films and gold-nanoparticles-doped films.[8] Poly(9,9-dioctylfluorene-*co*-benzothiadiazole) (F8BT), a conjugated polymer commonly used in organic light-emitting diodes (OLEDs), is used as the active material that generates ECL.[9] The ECL waves are launched by intentional scratches which provide leaks or embedded gold nanoparticles (Au NPs) that offer leaks or electric shorts.[8] Several stages for the transport mechanism of ECL soliton waves were proposed, including the formation of the local electrochemical double layer, the

J.-T. Chen
Department of Applied Chemistry, National Chiao Tung University, Hsinchu 30050, Taiwan
Fax: (886)-3-5131523; E-mail: jtchen@mail.nctu.edu.tw
J.-T. Chen, Y.-L. Chang, S. Guo, O. Fabian, W. M. Lackowski, P. F. Barbara
Department of Chemistry and Biochemistry, Center for Nano- and Molecular Science and Technology, The University of Texas at Austin, Austin, Texas 78712, USA

[a] Supporting information for this article is available at the bottom of the article's abstract page, which can be accessed from the journal's homepage at http://www.mrc-journal.de, or from the author.

DOI: 10.1002/marc.201000747

oxidation of polymers followed by solvent-swelling of polymer films, and further transport of anions and solvent that advances the double layer with the ECL wavefront. The study of ECL wave provides a new and unique way to investigate the oxidation front phenomenon in conjugated polymer films.[10,11] In spite of this, the controlling factors of the soliton-like ECL wave process such as polymer film thickness and composition must be further investigated in order to gain more insight and understand deeper about the ECL wave mechanism. In addition, it is necessary to study how the spatial distribution of the ECL depends on the morphology of polymers.

Here we report a more detailed study of soliton-like ECL waves from pure polymer films and gold-nanoparticles-doped polymer films by changing factors such as film thickness and distribution of local leaks. For thinner (≈15 nm), pure F8BT films, dendritic ECL filaments are generated from many cracks in the film after applying the electrochemical potential.

For thicker (≈250 nm), pure F8BT films, ECL waves are launched by natural defects or artificial scratches after applying an appropriate electrochemical potential. In addition to pure polymer film, we also apply the ECL wave phenomenon to polymer blends of conjugated and non-conjugated polymers to investigate how the ECL behavior depends on the composition, morphology, and solubility of polymer films. When F8BT is blended with polystyrene (PS), less soluble in the electrolyte solution, dotted ECL waves are observed. When F8BT is blended with poly(methyl methacrylate) (PMMA), more soluble in the electrolyte solution, ECL is launched simultaneously from many PMMA domains that act as local leaks where double layers are formed.

We use a simple ionic cluster model to describe the phenomenon of ECL waves. When the polymers get oxidized from local leaks, the anions (ClO_4^-) diffuse into the polymer film to maintain the charge neutrality.[12] At the same time, the solvent molecules accompany the anions into the film to avoid the loss of the solvation energy. Therefore a cluster of hole, anion, and solvent molecules are formed and diffuse through the oxidized/nonoxidized (wet/dry) interface. The advancing of this wet/dry interface is controlled by the diffusion kinetics in which the diffusion constant is a function of the concentration of the ions.[13,14]

Experimental Part

Materials

Poly(9,9-dioctylfluorene-*co*-benzothiadiazole) (F8BT) ($\overline{M}_w$: 70 kg · mol^{-1}) was purchased from American Dye Source. PS ($\overline{M}_w$: 106 kg · mol^{-1}) was received from Polymer Source. PMMA ($\overline{M}_w$: 101 kg · mol^{-1}) and Lithium perchlorate ($LiClO_4$) were obtained from Sigma–Aldrich. Tri-*n*-propylamine (TPA) and acetonitrile (MeCN) were purchased from Acros. ITO substrates were obtained from Metavac. Silver wires (25 μm in diameter) were purchased from Goodfellow.

Sample Preparation

15, 50, and 250 nm-thick F8BT films are made by spin-coating 150 μL F8BT solutions with concentration of 1.4, 14, and 28 mg · mL^{-1} in toluene, respectively onto cleaned ITO substrates at 2 000 rpm for 60 s. Au-NPs-doped F8BT films were made by spin-coating 150 μL Au NPs solution (250 nm colloids in water, BBInternational) at 2 000 rpm for 60 s followed by spin-coating 150 μL F8BT solution (14 mg · mL^{-1} in toluene) at 2 000 rpm for 60 s onto ITO substrates. Films of polymer blends (F8BT/PS or F8BT/PMMA) were made by spin-coating 150 μL polymer blend solutions with different ratios onto the ITO substrate. For example, solution of F8BT/PS (F8BT/PS = 1:4 w/w) was made by mixing 11.4 mg of F8BT with 44.8 mg of PS into 1 mL of toluene followed by spin-coating 150 μL solution onto the ITO glass at 2 000 rpm for 60 s. The thickness of the polymer films was measured by atomic force microscopy (AFM) as follows: the polymer film was first scratched by a near-field scanning optical microscopy tip (size ≈50 μm). Then the thickness of the polymer film was extracted from the cross sections of the AFM scans across the scratch.

Electrogenerated Chemiluminescence (ECL) Cell Fabrication

The fabrication process and configuration of ECL cells were described previously in more detail.[15] The configuration of the EC cell is shown in the Supporting Information. The MeCN solution contains 0.1 M electrolyte $LiClO_4$ and 0.1 M TPA. The scratches on the polymer films were generated by a near-field optical microscopy (NSOM) tip. The photoluminescence (PL) and ECL images were obtained by using a wide-field microscope (Nikon, Eclipse TE2000) and a CCD camera (Roper Scientific, Cascade 512B). The reported electrochemical potentials related to Quasi reference electrode (QRE) were provided by a potentiostat (Autolab, PGSTAT 100). For ferrocenium/ferrocene (Fc/Fc^+) couple internal standard, the electrochemical potentials were 0.20 ± 0.04 V more negative than those for QRE.

Results and Discussion

At first, we study the ECL behavior of thin (≈15 nm) and thick (≈250 nm) F8BT films. In our previous work, we have shown that the ECL waves can be launched from scratches or embedded nanoparticles (NPs) which provide leaks or shorts.[8] For the pure polymer film with the thickness of 15 nm, ECL starts immediately after applying the electrochemical potential without scratches or embedded NPs (Figure 1a–c). Dendritic ECL filaments are observed as a result of drying cracks that serve similar function as scratches or embedded NPs. The drying cracks are exposed to the electrolyte solution and the electrochemical double

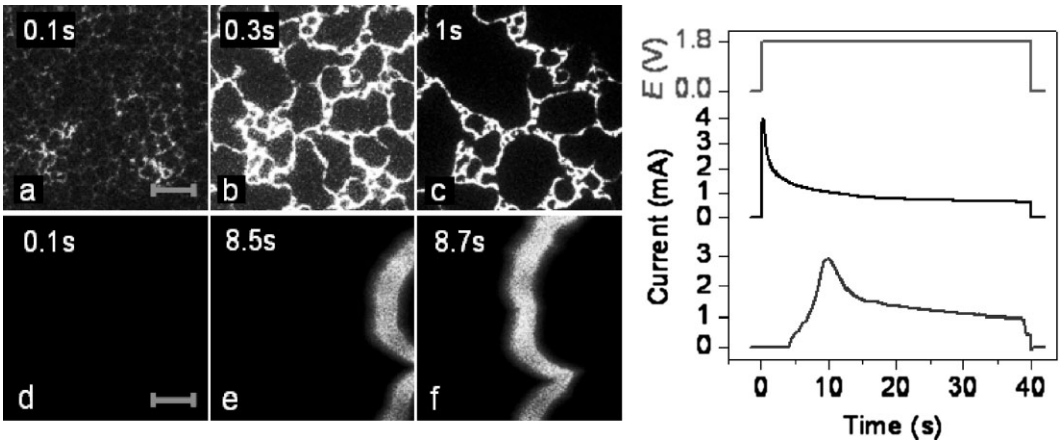

Figure 1. Electrogenerated chemiluminescence (ECL) images of thin (≈15 nm) and thick (≈250 nm) F8BT ($\overline{M}_w$: 70 kg · mol^{-1}) films in the MeCN solution of 0.1 M $LiClO_4$ and 0.1 M TPA. ECL images of the thin film at (a) 0.1, (b) 0.3, and (c) 1 s after the application of 1.8 V with the simultaneously measured current (middle curve) shown in the right panel. The applied electrochemical potential is shown as the top curve. (d–f) ECL images of the thick F8BT film at 0.1, 8.5, and 8.7 s after the application of 1.8 V with the current curve shown as the bottom curve in the right panel. The scale bars are (a) 15 and (d) 90 μm. The integration time for all images is 100 ms.

layers are formed in these leaked regions.[8] Thus, ECL is produced from these randomly located leaks. From the current versus time curves (middle curve in the right panel of Figure 1), the EC current rises sharply at the beginning when the electrochemical potential is applied, indicating the simultaneous oxidation of polymers and TPA from many localized leaks.

The ECL behavior of thicker polymer films (≈250 nm) is different from that of thin polymer films (≈15 nm). Without leaks in the polymer film, ECL is not promptly initiated because there are no paths for the anions and solvent molecules to form the double layer at the working electrode. When there is a local leak in the film, such as a natural defect or an artificial scratch, the anions and solvent molecules can penetrate the polymer film and access the working electrode. The anions and solvent molecules can reach the working electrode to form an electrochemical double layer while an electrochemical potential is applied. If a high enough electrochemical potential is applied (> 1.5 V), both polymer and TPA are oxidized and form $F8BT^{\cdot+}$ and $TPA^{\cdot}$, respectively. The electron transfer reaction between $F8BT^{\cdot+}$ and $TPA^{\cdot}$ produces the excited state molecules which decay to the ground state with emission of light. Consequently, oxidation of the polymer is triggered at the leaks, and an ECL wave is initiated, promoting the transport of the electrolyte ions. Figure 1d–f show the ECL images of a thick (≈250 nm) polymer film at 0.1, 8.5, and 8.7 s after applying an electrochemical potential of 1.8 V. No ECL is observed immediately after the application of 1.8 V because of the lack of defects at the observed region. After 8.5 s, an ECL wave propagates into the observed region, presumably from an out-of-region natural defect. The current versus time curve of the thick film (≈250 nm) sample is shown as the bottom curve in the right panel of Figure 1. No appreciable current is measured until 4 s after the application of 1.8 V when a small amount of polymer is oxidized at the out-of-region defects. The EC current rises gradually with time, indicating the expanding regions of oxidized polymer. The irregular shape of the ECL wave might be due to the collision and merging of several ECL waves or the local heterogeneity of the polymer film.

In addition to drying cracks, intentional scratches, or natural defects, ECL waves can also be launched by Au NPs, which is demonstrated in the case of gold-nanoparticles-doped F8BT films. Spatially separated Au NPs are first spread onto the ITO glass followed by the spin-coating of F8BT solutions. The size of the Au NPs (≈250 nm) is much larger than the thickness of the polymer film (≈50 nm) and Au NPs are exposed to the electrolyte solution before the application of the electrochemical potential. Each conductive Au NP acts as a small, extended electrode, or provides a leak at the F8BT/Au NP interface.[8] In our previous report, we have demonstrated that the ECL waves can be triggered by gold-nanoparticles-doped in F8BT films.[8] However, it is still not clear if the ECL waves are actually starting from the locations of the NPs. Also, we would like to know if ECL waves initiated from Au NPs are all propagating waves. Figure 2a shows the PL image of the F8BT film doped with Au NPs when the sample is excited by an Ar ion laser at 488 nm while no electrochemical potential is applied. Individual brighter spots indicate the locations of the Au NPs due to the local PL enhancement of F8BT film by surface plasmon (SP) resonance of Au NPs.[16] After applying the electrochemical potential in the absence of laser excitation, ECL waves are initiated at the F8BT/Au interface because of physical leaks or electrical shorts, as shown in Figure 2b–e.[8] Figure 2b shows the ECL image of the doped film at 0.1 s after applying an electrochemical potential of

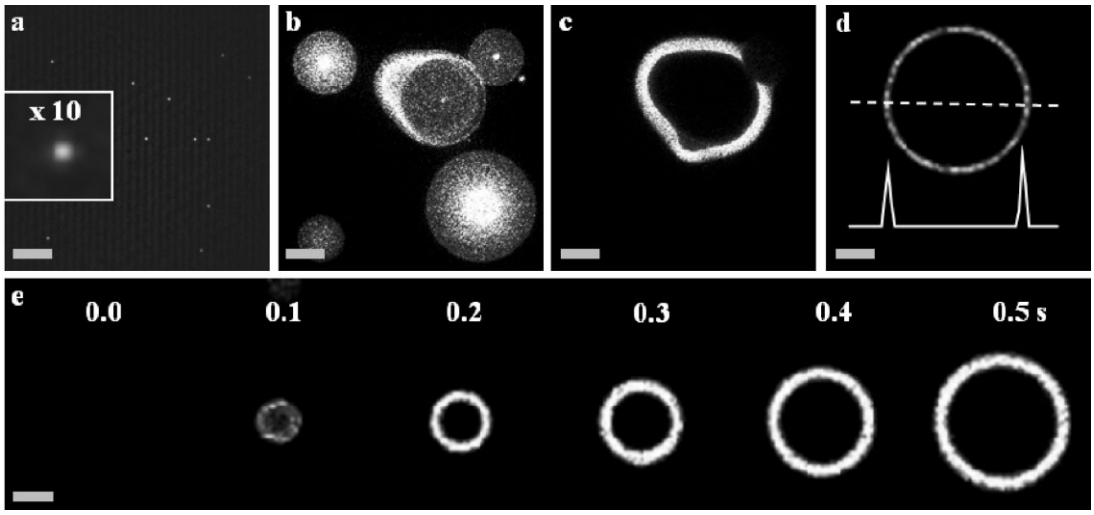

Figure 2. Photoluminescence (PL) and ECL images of F8BT films (≈50 nm, $\overline{M}_w = 70\ kg \cdot mol^{-1}$) doped with Au nanoparticles (diameter ≈250 nm) in an MeCN solution of 0.1 M $LiClO_4$ and 0.1 M TPA. The integration time for all images is 100 ms. (a) PL image of F8BT/Au NPs film. This image has been background-flattened and the inset shows ten times enlarged image of an Au NP. The corresponding ECL images at (b) 0.1 and (c) 0.2 s after the application of 1.8 V. (d) The ECL image of a sharp circle from an Au NP. The intensity scan along the dashed line is shown at the bottom of (d). (e) The ECL free wave initiated from an Au NP at different times after the application of 1.5 V. The wave speed in (e) is $\approx 55\ \mu m \cdot s^{-1}$. The scale bars are 10 μm in (a–c) and 20 μm in (d–e).

1.8 V. By comparing the PL and ECL images, we are able to show that ECL waves are really initiated from the Au NPs. In addition, our new results demonstrate more detail studies of the two types of ECL waves (i.e., pinned and free waves) that are initiated from Au NPs.[8] Some ECL waves are pinned and extinguish after a short time (<0.1 s) (from Figure 2b to c, some circular waves disappear). Figure 2c shows the ECL image after applying the electrochemical potential at 1.8 V for 0.2 s and only one free wave is observed to propagate outward. For the difference between pinned and free waves, we propose that there is an energy barrier to overcome for the ECL waves to propagate. Some waves are able to overcome the energy barrier and propagate. This energy barrier might be related to the presence of the co-reactant, TPA, which reduces back the oxidized polymers and keeps some F8BT in the dry state.

The line scan of a ring-shaped ECL wave initiated from an Au NP is shown in Figure 2d. The line scan indicates the narrow interfaces between the nonoxidized (i.e., ahead of the wavefront) and oxidized regions (i.e., behind the wavefront). The images of ECL triggered from a single Au NP at different times are shown in Figure 2e. The first image in Figure 2e shows the background image while the electrochemical potential is at 0 V and no ECL is observed. At 0.1 s, after the electrochemical potential steps to 1.5 V, a small disk-shaped ECL is formed. Later, a ring-shaped ECL propagates outward isotropically at a constant speed ($\approx 55\ \mu m \cdot s^{-1}$). The plot of radius versus time for the ECL waves shown in Figure 2e is displayed in Figure S3 in the Supporting Information. The circular shape of the ECL wave suggests that the film thickness, the swelling of the polymer, and the transport of the electrolyte solution are laterally uniform. The ECL waves propagate as rings with increasing sizes rather than disks because of the quenching by oxidized polymers and, ultimately, the irreversible reaction following the oxidation. This irreversible reaction of the F8BT has been described in our previous publications on F8BT NPs.[15,17,18]

To further understand how the composition and morphology of polymer films affects the oxidation-induced swelling and the resulting ECL wave kinetics, we study the blend systems of F8BT and another nonconjugated polymer, PS, with different composite ratios. Different ratios of the blends are used to control the distance between the light-emitting F8BT domains. PS is less soluble in MeCN than PMMA due to the difference of the solubility parameters. The solubility parameters of PS, PMMA, and MeCN are 9.1, 9.45, and 11.9 $(cal \cdot cm^{-3})^{1/2}$, respectively. The blended polymer film is phase-separated after spin-coating the polymer blend solution onto the ITO surface.[19] Figure 3 shows the PL and ECL images from polymer blend of F8BT and PS (F8BT/PS = 1:4 w/w), in which F8BT is the minor domain surrounded by the major PS domain. Figure 3a shows the PL image of the F8BT/PS blend after the excitation by an Ar ion laser at 488 nm, showing the fluorescent F8BT domains. After applying the electrochemical potential at 1.6 V in the absence of the laser excitation, dotted ECL waves are observed to propagate, presumably from the scratched region that is out of the observed region. In Figure 3d–i, the wave of dotted-ECL propagates across the observed region from the lower right corner to the upper left corner. The wave speed ($\approx 30\ \mu m \cdot s^{-1}$) is much slower compared

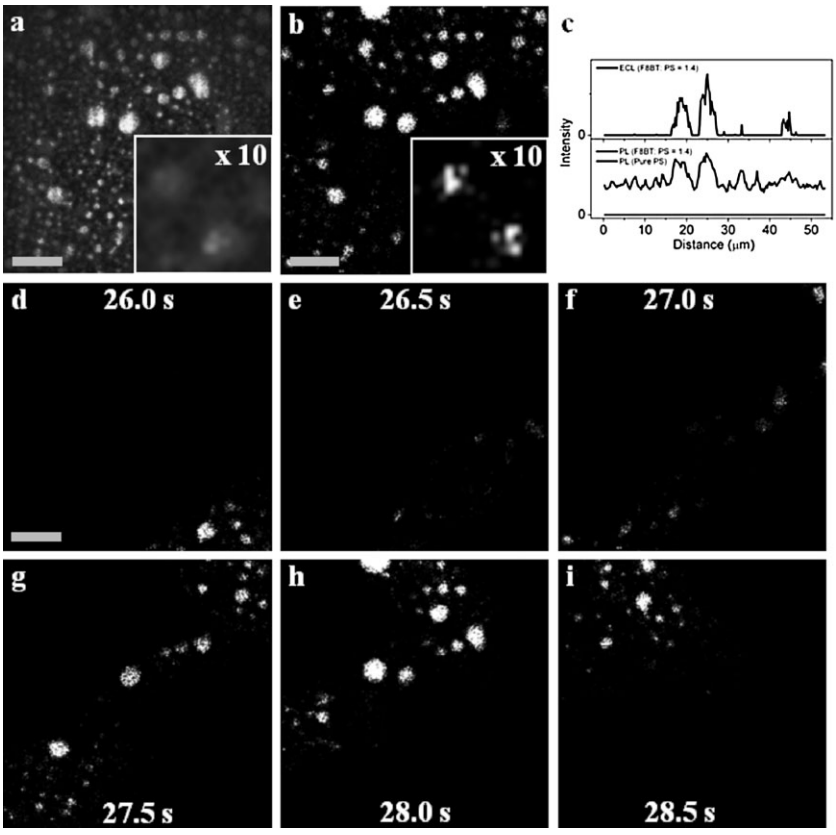

Figure 3. Photoluminescence (PL) and ECL images of F8BT/PS blend (F8BT/PS = 1:4 w/w, 56 mg · mL^{-1} in toluene) in an MeCN solution of 0.1 M $LiClO_4$ and 0.1 M TPA. The thickness of the polymer film is ≈300 nm. (a) The PL image which has been background-flattened. (b) The superimposed image from ECL images at 26–28.5 s (c) Line scans of PL and superimposed ECL images in (a) and (b). The line scan of PL from pure PS is shown in the bottom curve. (d–i) ECL images at different time frames after the application of 1.6 V. All scale bars are 10 μm. The integration times are 0.1 s in (a) and 0.5 s in (d–i). The wave speed is ≈30 μm · s^{-1}.

to the F8BT-only film (≈100–300 μm · s^{-1}) when the same electrochemical potential (1.6 V) is applied. The difference in speed is due to the presence of the resistant PS phase. Figure 3b is the summed ECL image from Figure 3d–i and main features of the F8BT domains are matched with the fluorescent domains shown in the PL image (Figure 3a).

It is interesting to learn that ECL waves can transport between adjacent F8BT domains because the host polymer (PS) should be less accessible to the electrolyte solution due to the poor solubility. Ion and solvents mostly diffuse into the F8BT domains to neutralize the oxidized polymers during the oxidation process. One possible explanation is that there are still some F8BT polymers present in the PS-rich domains for the electrolyte solution to transport. The presence of the F8BT polymers in the PS-rich domain is demonstrated in the line scan of the PL image (Figure 3c). Figure 3c also shows that main phase features of the polymer blend are matched in PL and ECL, but some domains shown in the PL images are not observed in the summed ECL image. These ECL-free regions might be isolated F8BT domains which are not accessible to the TPA radicals for producing ECL. Another possible reason for the transport of the ECL wave between the F8BT domains might be due to the presence of a thin wetting layer of F8BT near the ITO surface, which provides a pathway under the blend film. We also try to see if there are still oxidation waves for the blend films when no co-reactant, TPA, is used and ECL is not produced. We examine the oxidation waves by checking the PL quenching waves in which the sample is excited by the Ar ion laser and electrochemical potential is applied in the absence of TPA. As a result, oxidation waves are still observed in the PL quenching experiments. Therefore, the wave phenomena occur in both ECL and PL quenching experiments.

Another nonconjugated polymer, PMMA, is also used as the host polymer in F8BT blend systems to study how the solubility of the host polymer affects the ECL process. PMMA is more soluble in MeCN than PS, allowing electrolyte solutions to penetrate the PMMA domains and leaks are formed at the F8BT/PMMA interfaces. The double layer is promptly established at the working electrode when an electrochemical potential is applied. Figure 4 shows the results of the polymer blends composed of F8BT and PMMA (F8BT/PMMA = 1:1 w/w). More intense PL indicates F8BT-rich domains, as shown in Figure 4a. Figure 4b shows the ECL image at 1 s after applying 1.6 V. Unlike the F8BT/PS blends in which ECL transports as waves, ECL of F8BT/PMMA blends appears everywhere simultaneously after the electrochemical potential is applied. The electrolyte solution is able to diffuse into the soluble PMMA domains and each PMMA domain just acts like a scratch or a defect. The different ECL behavior between F8BT/PS and F8BT/PMMA blend is mainly due to the difference in solubility of the nonconjugated polymers. Figure 4c shows the line scans of PL and ECL images and PL and ECL are stronger in F8BT-rich domains. The thicknesses of the polymer films shown in Figure 3 and 4 are ≈300 and 40 nm, respectively. Note that the thickness of the polymer film might also affect the ECL behavior of the polymer blend films. In the future, we will study the morphologies of polymer blends or block copolymers with different thicknesses and their effects on the ECL behavior.

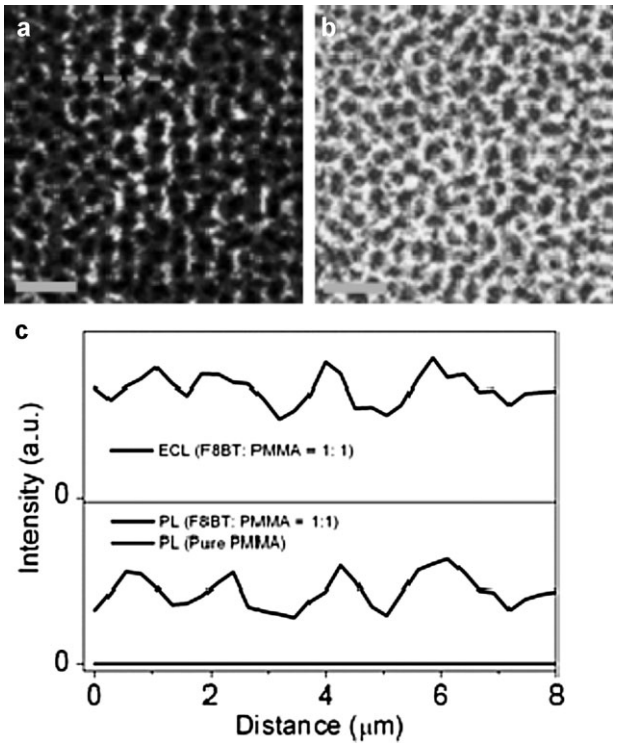

Figure 4. Photoluminescence (PL) and ECL images of polymer blends of F8BT and PMMA (F8BT/PMMA = 1:1 w/w, 7 mg · mL^{-1} in toluene) in an MeCN solution of 0.1 M $LiClO_4$ and 0.1 M TPA. Both images are acquired with an integration time of 100 ms and the scale bars are 5 μm. The thickness of the polymer film is ≈40 nm. (a) The PL image which has been background-flattened. (b) The ECL image after applying 1.6 V for 1 s. (c) Line scans for PL in (a) and ECL in (b). The line scan of PL from pure PMMA is also indicated as the bottom curve.

Conclusion

In conclusion, we study the ECL wave phenomenon from pure F8BT films and gold-nanoparticles-doped F8BT films in more detail and apply this phenomenon to polymer blends of conjugated and nonconjugated polymers. For the transport mechanism of ECL, we find that leaks or shorts are required to initiate ECL waves, which can be generated by using natural defects in films, making artificial scratches, embedding Au NPs, or mixing with PMMA polymers. These results are consistent with the proposed mechanism in which the direct contact of electrolyte ions and the working electrode is essential to trigger the EC reaction. Solubilities of the host polymers are found to play an important role for the ECL behavior of polymer blends. When F8BT is blended with PS, less soluble in the electrolyte solution, ECL can propagate as waves even in the PS-rich domains. On the contrary, ECL is produced ubiquitously for the blend of F8BT and PMMA, in which electrolyte ions are more accessible to the PMMA domains. For possible future work, we would like to study different effects on the ECL kinetics such as morphology, electrochemical potential, co-reactant concentration, and counterion concentration.

Acknowledgements: This work was supported by the *National Science Foundation*, the *Welch Foundation*, and the *National Science Council of Taiwan*.

Received: November 26, 2010; Revised: January 18, 2011; Published online: March 7, 2011; DOI: 10.1002/marc.201000747

Keywords: conjugated polymers; electrochemistry; nanoparticles; photoluminescence; polymer blends

[1] A. J. Bard, "*Electrogenerated Chemiluminescence*", Marcel Dekker, New York 2004.
[2] W. J. Miao, *Chem. Rev.* **2008**, *108*, 2506.
[3] N. R. Armstrong, R. M. Wightman, E. M. Gross, *Annu. Rev. Phys. Chem.* **2001**, *52*, 391.
[4] P. Bertoncello, R. J. Forster, *Biosens. Bioelectron.* **2009**, *24*, 3191.
[5] I. Prieto, J. Teetsov, M. A. Fox, D. A. V. Bout, A. J. Bard, *J. Phys. Chem. A* **2001**, *105*, 520.
[6] M. M. Richter, F. R. F. Fan, F. Klavetter, A. J. Heeger, A. J. Bard, *Chem. Phys. Lett.* **1994**, *226*, 115.
[7] M. R. Warren, J. D. Madden, *J. Electroanal. Chem.* **2006**, *590*, 76.
[8] Y. L. Chang, R. E. Palacios, J. T. Chen, K. J. Stevenson, S. Guo, W. M. Lackowski, P. F. Barbara, *J. Am. Chem. Soc.* **2009**, *131*, 14166.
[9] A. C. Morteani, P. Sreearunothai, L. M. Herz, R. H. Friend, C. Silva, *Phys. Rev. Lett.* **2004**, *92*, 4.
[10] Y. Tezuka, S. Ohyama, T. Ishii, K. Aoki, *Bull. Chem. Soc. Jpn.* **1991**, *64*, 2045.
[11] X. Z. Wang, B. Shapiro, E. Smela, *Adv. Mater.* **2004**, *16*, 1605.
[12] T. F. Otero, H. Grande, J. Rodriguez, *Synth. Met.* **1996**, *83*, 205.
[13] J. J. L. Cascales, T. F. Otero, *J. Chem. Phys.* **2004**, *120*, 1951.
[14] I. J. Suarez, T. F. Otero, M. Marquez, *J. Phys. Chem. B* **2005**, *109*, 1723.
[15] R. E. Palacios, F. R. F. Fan, A. J. Bard, P. F. Barbara, *J. Am. Chem. Soc.* **2006**, *128*, 9028.
[16] M. S. Kim, D. H. Park, E. H. Cho, K. H. Kim, Q. H. Park, H. Song, D. C. Kim, J. Kim, J. Joo, *ACS Nano* **2009**, *3*, 1329.
[17] Y. L. Chang, R. E. Palacios, F. R. F. Fan, A. J. Bard, P. F. Barbara, *J. Am. Chem. Soc.* **2008**, *130*, 8906.
[18] R. E. Palacios, W. S. Chang, J. K. Grey, Y. L. Chang, W. L. Miller, C. Y. Lu, G. Henkelman, D. Zepeda, J. Ferraris, P. F. Barbara, *J. Phys. Chem. B* **2009**, *113*, 14619.
[19] J. S. Kim, P. K. H. Ho, C. E. Murphy, R. H. Friend, *Macromolecules* **2004**, *37*, 2861.